Studying Nonlinear Dynamical Systems on a Reconfigurable Analog Platform

K. Odame, C.M. Twigg, A. Basu, P. E. Hasler
School of Electrical and Computer Engineering
Georgia Institute of Technology, Atlanta, Georgia 30332–0250
odame@ece.gatech.edu

***Abstract*— We have developed a field programmable analog array (FPAA) that can be configured to synthesis and analyze a vast variety of circuits. This FPAA is a valuable platform for studying nonlinear dynamics in circuits, as it offers close to the flexibility of computer simulation, but with actual experimental results. We present data from a current mirror, a peak detector, and a second-order section.**

I. Enabling a Nonlinear Paradigm with an FPAA

Portable and implantable, always-on electronics stand to benefit from analog signal processing, when only low levels of precison are necessary [1, 2]. To achieve sophisticated signal processing with low power and area overhead, analog processors must exploit fundamental nonlinear dynamics that are found in devices and simple circuits. So, the analog designer must depart from the traditional linear design paradigm, and learn to analyze and understand circuits from a nonlinear dynamical systems theory perspective. Transient simulation is a first step to understanding circuit dynamics, but it is probably more desirable to get hardware results of circuit behavior.

We have developed a field programmable analog array (FPAA) that can be configured to synthesis and analyze a vast variety of circuits [3]. Figure 1 depicts a simple, second-order filter compiled on our FPAA. More complex circuit configurations are possible, and would involve a larger number of the over 400 components in the FPAA. In this paper we demonstrate the utiltity and versatility of the FPAA in analyzing the dynamics of a number of fundamental circuit blocks.

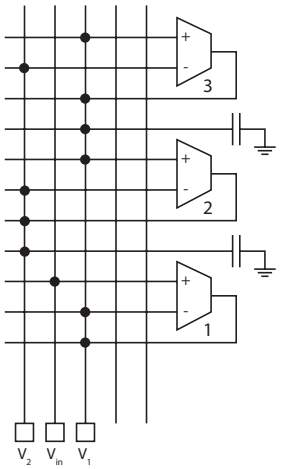

Fig. 1. Compiled Circuit on an FPAA. Component terminals can be connected or disconnected using the switch matrix. In this illustration, connections are indicated by solder dots. The gain of each amplifier is programable over a continuous range of values over a few decades.

II. One-Dimensional Systems

A. Simple Current Mirror

From KCL, the current mirror of Fig. 2 (a) obeys the following differential equation.

$$I_{\rm out} = C\frac{dV_{\rm out}}{dt} + I_{\rm b}. \tag{1}$$

Assuming subthreshold operation, (1) becomes

$$\tau\frac{dI_{\rm out}}{dt} \;=\; I_{\rm out}\left(1 - \frac{I_{\rm out}}{I_{\rm b}}\right), \tag{2}$$

where $\tau = (\kappa I_{\rm b})/(CU_{\rm T})$, with κ being the body effect coefficient and $U_{\rm T}$ the thermal voltage. For a fixed value of $I_{\rm b}$, (2) happens to be the *logistic equation*, a simple model of population dynamics. $I_{\rm out}$ corresponds to the population size. $I_{\rm b}$ is the carrying capacity, and $I_{\rm b}/(4\tau)$ is the maximum growth rate.

The logistic equation can be solved exactly either by separation of variables followed by partial fractions, or by solving it as Bernoulli's equation. The solution is

$$I_{\rm out}(t) = \frac{I_{\rm b}e^{t/\tau}}{e^{t/\tau} - 1 + I_{\rm b}/I_{\rm out_0}}, \tag{3}$$

where $I_{\rm out_0}$ is the initial value of $I_{\rm out}$. We are lucky to have an exact solution to (2), given that it is a nonlinear differential equation. Even so, it is difficult to discern much useful information about $I_{\rm out}$'s qualitative behavior from (3).

1) Geometric Analysis using the FPAA: To better understand the current mirror's large-signal behavior, we compiled it on the FPAA and measured its response to various step inputs. Each input step ends at a value of $I_{\rm b} = 5$nA. These measurements are depicted as the solution curves of Fig. 2 (b). With these, we created the vector field of $dI_{\rm out}/dt$ versus $I_{\rm out}$, Fig. 2 (c).

The value of $I_{\rm out}$ is increasing for positive values of $dI_{\rm out}/dt$, decreasing for negative values of $dI_{\rm out}/dt$ and constant at the x-intercepts. The fixed points are $I_{\rm out} = 0$ and $I_{\rm out} = I_{\rm b}$. To the right of $I_{\rm out} = 0$, the value of $dI_{\rm out}/dt$

1-4244-0921-7/07 $25.00 © 2007 IEEE.

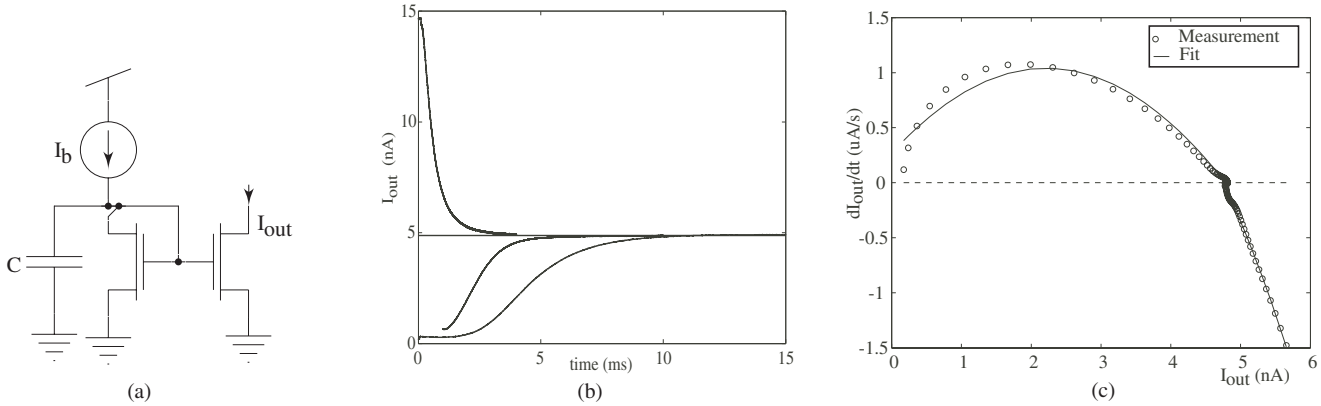

Fig. 2. Simple Current Mirror. (a) Circuit that was compiled onto the FPAA. (b) Measured step responses. (c) Vector field derived from step response measurements. The origin is an unstable fixed point, while $(0, 5)$ is stable.

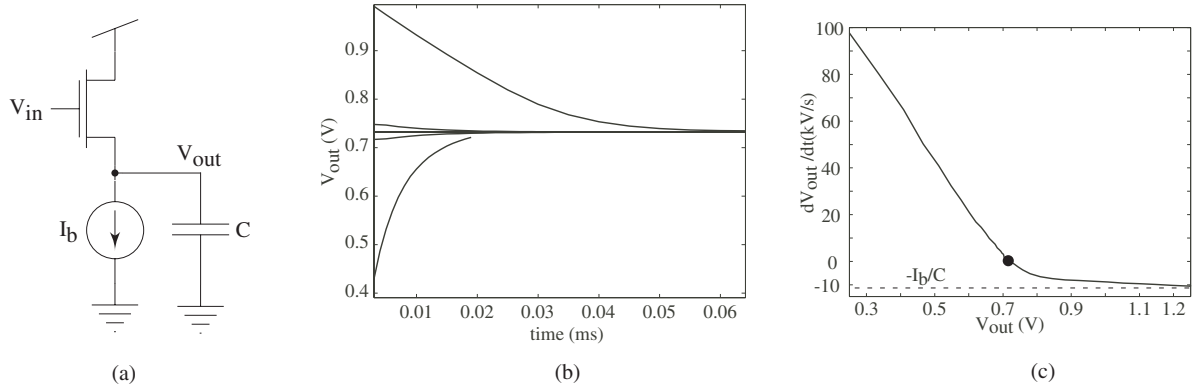

Fig. 3. Source Follower Amplifier Acting as a Simple Peak Detector. (a) Circuit that was compiled onto the FPAA. (b) Measured step responses. (c) Vector field derived from step response measurements. The point $(0, 0.7)$ is a stable fixed point.

is positive. This implies that a slightly nonzero value of $I_{\rm out}$ will grow. In fact, any nonzero value of $I_{\rm out}$ will grow, as long as it is less than $I_{\rm b}$. For $I_{\rm out} > I_{\rm b}$, $I_{\rm out}$ will decrease, since $dI_{\rm out}/dt < 0$. So, values of $I_{\rm out} = I_{\rm b}^-$ and $I_{\rm out} = I_{\rm b}^+$ both flow towards the $I_{\rm out} = I_{\rm b}$ fixed point, indicating that it is a stable fixed point. As $I_{\rm out} = 0^+$ flows away from $I_{\rm out} = 0$, it is an unstable fixed point.

While Fig. 2 (c) is no substitute for the quantitative information represented in (3), it still reveals important information about the current mirror's behavior. For instance, any nonzero value of $I_{\rm out}$ that is less than $I_{\rm b}/2$ will grow with increasing speed, reaching its largest growth rate of $I_{\rm b}/(4\tau)$ at $I_{\rm out} = I_{\rm b}/2$. Then, the growth rate of $I_{\rm out}$ will start to decrease, until it decays to zero, at which point $I_{\rm out} = I_{\rm b}$. For $I_{\rm out} > I_{\rm b}$, however, the speed at which $I_{\rm out}$ approaches $I_{\rm b}$ is always reducing. That is, the maximum rate of decay depends on the initial condition, $I_{\rm out_0}$, for all $I_{\rm out_0} > I_{\rm b}$, while the growth rate is bounded by $I_{\rm b}/(4\tau)$ for $I_{\rm out_0} < I_{\rm b}$.

B. Simple Peak Detector

Assuming subthreshold operation, the KCL equation for the source follower amplifier of Fig. 3 (a) is the following.

$$C\frac{dV_{\rm out}}{dt} = I_{\rm o}e^{(\kappa V_{\rm in} - V_{\rm out})/U_{\rm T}} - I_{\rm b}. \tag{4}$$

Note that

$$\frac{d}{dt}e^{V_{\rm out}/U_{\rm T}} = \frac{e^{V_{\rm out}/U_{\rm T}}}{U_{\rm T}}\frac{dV_{\rm out}}{dt}, \tag{5}$$

in which case, the solution to (4) is

$$V_{\rm out} = \kappa V_{\rm in} + U_{\rm T}\log\left(\frac{I_{\rm o}}{I_{\rm b}} - \left(\frac{I_{\rm o}}{I_{\rm b}} - e^{(V_{\rm out_0} - \kappa V_{\rm in})/U_{\rm T}}\right)e^{-t/\tau}\right), \tag{6}$$

where $\tau = CU_{\rm T}/I_{\rm b}$ and $V_{\rm out_0}$ is the initial value of $V_{\rm out}$.

The time that it takes for $V_{\rm out}$ to be within 10% of its final value is

$$t_{10} = \tau\log\left|\frac{I_{\rm o}/I_{\rm b} - e^{(V_{\rm out_0} - \kappa V_{\rm in})/U_{\rm T}}}{I_{\rm o}/I_{\rm b} - e^{0.1\kappa V_{\rm in}/U_{\rm T}}}\right|. \tag{7}$$

For a large positive step input, $e^{(V_{\mathrm{out}_0}-\kappa V_{\mathrm{in}})} \approx 0$, and (7) is approximately

$$t_{10} = t_{10+} \approx \tau \log \left| \frac{I_{\mathrm{o}}}{I_{\mathrm{o}} - I_{\mathrm{b}} e^{0.1\kappa V_{\mathrm{in}}/U_{\mathrm{T}}}} \right|. \tag{8}$$

For a large negative step input, $e^{(V_{\mathrm{out}_0}-\kappa V_{\mathrm{in}})} \gg I_{\mathrm{o}}/I_{\mathrm{b}}$, and (7) becomes

$$\begin{aligned} t_{10} = t_{10-} &\approx \tau \log \left| \frac{I_{\mathrm{b}} e^{(V_{\mathrm{out}_0}-\kappa V_{\mathrm{in}})}}{I_{\mathrm{o}} - I_{\mathrm{b}} e^{0.1\kappa V_{\mathrm{in}}/U_{\mathrm{T}}}} \right| \\ &= t_{10+} + \tau \left(\frac{V_{\mathrm{out}_0}}{U_{\mathrm{T}}} - \kappa \frac{V_{\mathrm{in}}}{U_{\mathrm{T}}} \right) \log \left(\frac{I_{\mathrm{b}}}{I_{\mathrm{o}}} \right). \end{aligned} \tag{9}$$

(8) and (9) indicate that the response of the peak detector is slower for a negative input step than it is for a positive input step. We surmise that if the input is continuously varying at a rate faster than $1/(t_{10-})$, then the output will be a reasonable representation of the input's peak values. Explaining the peak detector's behavior with (8) and (9) is rigorous, but depends on having to manipulate the expression of (6).

One way of avoiding the math is to employ intuitive descriptions of the charging action of the active device (i.e. the transistor) versus the discharging action of the current source [4]. A more rigorous approach is to apply nonlinear geometric analysis to the problem. Consider the plot of dV_{out}/dt versus V_{out} shown in Fig. 3 (c). We constructed it from a number of step response measurements that we took after compiling the source-follower amplifier onto the FPAA. A large negative input step corresponds to an initial value of $V_{\mathrm{out}_0} \gg V_{\mathrm{in}}$. The rate of growth of V_{out} is bounded by I_{b}/C. For a large positive input step, however, $V_{\mathrm{out}_0} \ll V_{\mathrm{in}}$, and the maximum rate at which V_{out} approaches V_{in} can be much greater than I_{b}/C. The maximum rate of approach in this case is limited only by the initial value, V_{out_0}. As such, there is an asymmetry in the speed of the circuit's response to up-going versus down-going movements on the input. The effect of this asymmetry is that V_{out} tracks increasing V_{in} and not decreasing V_{in}, which is the behavior of a peak detector.

III. A Two-Dimensional System

Figure 4 depicts Lyon and Mead's classic second order section [5]. It is a Gm-C filter with two poles that can be placed anywhere on the real/imaginary plane. We begin our analysis by writing down the governing equations for the circuit, assuming that the OTAs are based on subthreshold MOS transistor differential pairs.

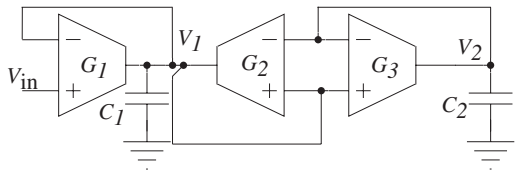

Fig. 4. Second Order Section. Varying the bias currents of the various amplifiers leads to interesting dynamics.

$$C_1 \frac{dV_2}{dt} = \frac{I_2}{k} \tanh\left(\frac{\kappa(V_1 - V_2)}{2U_{\mathrm{T}}} \right), \tag{10}$$

$$C_1 \frac{dV_1}{dt} = I_1 \tanh\left(\frac{\kappa(V_{\mathrm{in}} - V_1)}{2U_{\mathrm{T}}} \right) - I_3 \tanh\left(\frac{\kappa(V_2 - V_1)}{2U_{\mathrm{T}}} \right), \tag{11}$$

where $I_{1,2,3}$ are the bias currents of the OTAs. Also, k is the ratio of the C_2 to C_1.

If we define

$$x = \frac{\kappa(V_1 - V_{\mathrm{in}})}{2U_{\mathrm{T}}}, \qquad y = \frac{\kappa(V_2 - V_1)}{2U_{\mathrm{T}}}, \tag{12}$$

then (11) and (10) become

$$\begin{aligned} \frac{2U_{\mathrm{T}}C_1}{\kappa}\frac{dx}{dt} &= -I_1 \tanh(x) - I_3 \tanh(y) \\ \frac{2U_{\mathrm{T}}C_1}{\kappa}\frac{dy}{dt} &= I_1 \tanh(x) + \left(I_3 - \frac{I_2}{k} \right) \tanh(y). \end{aligned} \tag{13}$$

Further defining

$$\begin{aligned} I_1 &= I_{\mathrm{bias}} \\ I_2 &= gkI_{\mathrm{bias}} \\ I_3 &= 2rI_{\mathrm{bias}} \\ t &= \tau \cdot \frac{2U_{\mathrm{T}}C_1}{\kappa I_{\mathrm{bias}}}, \end{aligned}$$

where $g \geq 0$, we get the following dimensionless equation

$$\begin{aligned} \frac{dx}{d\tau} &= -\tanh(x) - 2r \tanh(y) \\ \frac{dy}{d\tau} &= \tanh(x) + (2r - g) \tanh(y). \end{aligned} \tag{14}$$

A. Small Signal Analysis

We can linearize (14) by replacing the RHS with its Jacobian, giving

$$\begin{bmatrix} \dot{x} \\ \dot{y} \end{bmatrix} \approx \begin{bmatrix} -1 & -2r \\ 1 & 2r - g \end{bmatrix} \begin{bmatrix} x \\ y \end{bmatrix} \tag{15}$$

The origin is a fixed point. In fact, it is a unique fixed point, since (from (14)) $\tanh(x) = -2r \tanh(y) \implies x = y = 0$. The origin is stable for

$$r < \frac{1+g}{2}, \tag{16}$$

and unstable otherwise. It is a spiral for

$$\frac{1+g}{2} - \sqrt{g} < r < \frac{1+g}{2} + \sqrt{g}, \tag{17}$$

and a node otherwise.

B. Large Signal Analysis

For certain values of r and g, the nonlinearities of the second-order section causes it to suffer instability. In this region of parameter space, linear analysis accurately predicts that the circuit is *small signal stable*, but completely fails to recognize that instability would occur for *large signals*. Mead addresses this issue in [6], but we will present a somewhat

more thorough treatment of the problem, using phase-plane analysis and experimental verification with the FPAA.

For very large values of x and y, the $\tanh$ functions get saturated, and can each be approximated with a signum function. (14) becomes

$$\begin{aligned} \frac{dx}{d\tau} &= -\mathrm{sgn}(x) - 2r\mathrm{sgn}(y) \\ \frac{dy}{d\tau} &= \mathrm{sgn}(x) + (2r-g)\mathrm{sgn}(y). \end{aligned} \tag{18}$$

Figure 5 shows the phase plane (x versus y) that corresponds to (18). The depicted motion is valid only if $1/2 < r < 1$. The gradient in the first and third quadrants is

$$a = \frac{2r-1+g}{1+2r},$$

and that in the second and fourth quadrants is

$$b = \frac{2r-1-g}{1-2r}.$$

Observe that, with an initial condition of $(1,0)$, (18) predicts

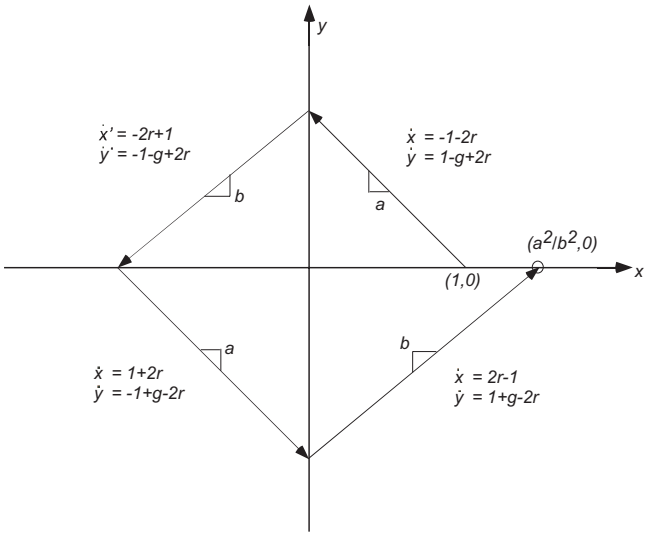

Fig. 5. Sketch of SOS Phase Plane for Large Signals

that the positive x-axis will again be intercepted at $(a^2/b^2, 0)$. If $a^2/b^2 > 1$, then x and y will grow without bound. Stated in terms of the r and g variables, there is large signal instability if

$$r > \frac{g+\sqrt{g^2+4}}{4}. \tag{19}$$

Our analysis of the second-order section can readily be verified experimentally. We compiled the filter on the FPAA, as shown in Fig. 1. The bias currents of all three OTAs are user-programmable, and varying them corresponds to varying the values of r and g. The FPAA thus allows us to explore the parameter space of the filter, and to observe changes in its qualitative behavior. It can effectively be used for bifurcation analysis.

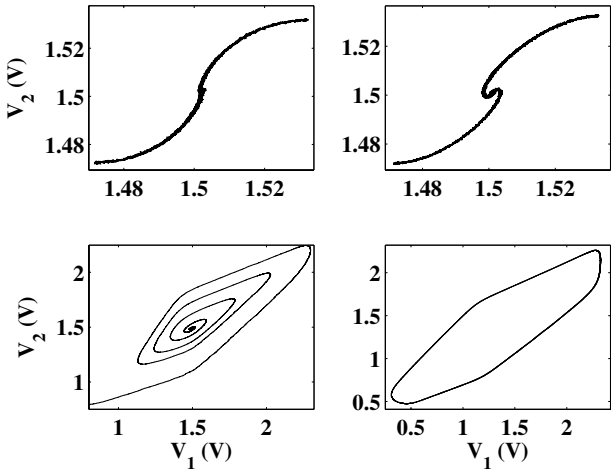

Fig. 6. SOS Experimental Phase Plane Results for Various Values of r.

Figure 6 shows the filter's phase plane plots for various values of r, with g kept fixed. Just as we predicted, there is a unique fixed point, which is initially stable, and gradually changes from a node to a spiral (top and bottom left panels of Fig. 6). While linear analysis would predict these three responses as damped, slightly underdamped, and very underdamped, it fails to recognize the possibility of the fourth response, which is large-signal instability. In the fourth panel, r meets the criterion derived from nonlinear analysis, (19), and we observe oscillation. Further analysis and exploration of parameter space reveals that this second-order section is capable of low-distortion sinusoidal oscillation [7]. Such functionality is valuable in communication systems.

IV. Conclusion

In this paper, we have introduced an FPAA as a viable tool for analyzing nonlinear circuit dynamics, and have supported our argument with experimental results for a few simple circuits. Future publications will involve more complex circuits, with several state variables and possibly chaotic behavior.

References

[1] R. Sarpeshkar, M.W. Baker, C.D. Salthouse, J.-J Sit, L Turicchia, and S.M. Zhak, "An analog bionic ear processor with zero-crossing detection," in *Proc. ISSCC'05*, Feb 2005, pp. 78–79.

[2] F. Serra-Graells, L. Gomez, and J.L. Huertas, "A true 1v 300w cmos subthreshold log-domain hearing-aid-on chip," *IEEE J. Solid-State Circuits*, vol. 39, no. 8, pp. 1271–1281, 2004.

[3] C. M. Twigg and P. E. Hasler, "A large-scale reconfigurable analog signal processor (rasp) ic," in *Proc. IEEE Custom Integrated Circuits Conference, CICC'06*, Sep 2006, pp. 5–8.

[4] B.P. Lathi, *Modern Digital and Analog Communication Systems*, Oxford University Press, New York, NY, 1998.

[5] R.F. Lyon and C. Mead, "An analog electronic cochlea," *IEEE Trans. on Acoustics, Speech and Signal Proc.*, vol. 36, no. 7, pp. 1119–1134, 1988.

[6] Carver Mead, *Analog VLSI and Neural Systems*, Addison-Wesley Publishing Company, 1989.

[7] K. Odame and P. Hasler, "Exploiting ota nonlinearity in the design of a second order section oscillator," in *Proc. RISP International Workshop on Nonlinear Circuits and Signal Processing, 2006*, Mar 2006, pp. 5–8.